POLITECNICO DI TORINO
Repository ISTITUZIONALE

Analysis of Electric Fault in a MV DC MgB2 Transmission Line Cooled by Liquid Hydrogen

Original
Analysis of Electric Fault in a MV DC MgB2 Transmission Line Cooled by Liquid Hydrogen / Cavallucci, L., Breschi, M., Macchiagodena, A., Mangiulli, G., Bracco, M., Farinon, S., Musenich, R., Savoldi, L.. - In: IEEE TRANSACTIONS ON APPLIED SUPERCONDUCTIVITY. - ISSN 1051-8223. - 36:5(2026), pp. 1-6. [10.1109/tasc.2026.3655642]

Availability:
This version is available at: 11583/3007605 since: 2026-02-14T17:40:45Z

Publisher:
Institute of Electrical and Electronics Engineers Inc.

Published
DOI:10.1109/tasc.2026.3655642

Terms of use:

This article is made available under terms and conditions as specified in the corresponding bibliographic description in the repository

Publisher copyright

(Article begins on next page)

30 October 2026

Analysis of Electric Fault in a MV DC MgB_2 Transmission Line Cooled by Liquid Hydrogen

Lorenzo Cavallucci, *Member, IEEE*, Marco Breschi, *Senior Member, IEEE*, Antonio Macchiagodena, Giovanni Mangiulli, Michela Bracco, Stefania Farinon, Riccardo Musenich, and Laura Savoldi, *Senior Member, IEEE*

***Abstract*—A submarine superconducting cable for the hybrid transmission of electricity and liquid hydrogen from a wind and solar offshore plant is under investigation in the frame of a project funded by the Italian Ministry of University and Research. The DC MgB_2 line is designed to connect the 300 MW offshore plant to the Ravenna port (Italy), approximately 22 km away, at an operating voltage of 30 kV. In this work, an electric model based on a lumped-parameter circuit of a DC medium voltage (MV) line including a MgB_2 conductor is coupled with a fluid-dynamic model suited to simulate fast thermodynamic transients in liquid hydrogen.**

***Index Terms*—Medium voltage superconducting line, hydrogen, MgB_2, electric fault conditions.**

I. Introduction

A SUBMARINE superconducting line based on magnesium diboride (MgB_2) [1], [2] for the hybrid transmission of electricity and liquid hydrogen [3], [4] from a wind and solar offshore plant [5], [6], under design in the Adriatic Sea, in Italy, is under investigation in the frame of the "Tricheco" project founded by the Italian Ministry [7]. The superconducting line is designed to operate under DC conditions at 30 kV and 10 kA. The line is supposed to connect the 300 MW offshore plant to the Ravenna port, Italy, approximately 22 km away [8].

In previous works, the design of the transmission line and the analysis of the normal operating conditions have been presented [7], [9]. In this work, the off-normal conditions of the line during an electrical fault are investigated, whereas the off-normal conditions related to the cable cooling are addressed in a separate analysis [10]. The fault analysis of this DC medium voltage (MV) transmission line is critical for an appropriate design of its protection. It is important that this analysis accounts for both the electrical and hydraulic aspects, as faults can create interactions between the superconducting cable electrical behavior and the pressurized hydrogen system. Understanding these interactions is important to guarantee the safety, reliability, and quick fault isolation of the transmission line. Fault conditions in these lines can arise due to various factors, such as the degradation of the insulation and the occurrence of overcurrent or short circuits.

Several works have recently been published describing coupled electrical and thermal circuit models for the simulation of fault conditions in superconducting transmission lines [11], [12], [13]. In most of these works, the fluid-dynamic behavior of the coolant is not modeled. This represents one the main novelty of this work. In this work, an electric model based on a lumped-parameter circuit of a DC MV line including a MgB_2 conductor is coupled with a fluid dynamic model suited to simulate the thermodynamic transients in liquid hydrogen. The coupled electrical and fluid-dynamic model is applied to simulate a pole-to-ground fault of the MV DC line.

Different cable designs and transmission line layouts are analyzed. In the first cable design, MgB_2 wires are arranged around a former and assembled with highly conductive metal wires. This layout results in higher thermal inertia of the cable but also leads to lower electrical resistance. The tradeoff between these two contributions is here investigated. In the second cable design, the former is absent, and the MgB_2 wires are arranged in a bundle without a copper former. This layout, in contrast, is characterized by lower thermal inertia and higher electrical resistance.

The first cable design represents the nominal configuration, whereas the second one is proposed primarily as a cost-reduction measure. This alternative layout has no impact on the design of other components of the cable.

Two layouts of the transmission lines are also presented. The first layout is a bipole line with a conventional normal-conducting return, see Table I for its geometry. The return is

Received 17 October 2025; revised 1 January 2026; accepted 13 January 2026. Date of publication 19 January 2026; date of current version 4 February 2026. This work was supported by Ministero dell'Università e della Ricerca, Italy –within the PRIN 2022 Program (D.D.104 -02/02/2022). *(Corresponding author: Lorenzo Cavallucci.)*

Lorenzo Cavallucci, Marco Breschi, and Antonio Macchiagodena are with the Department of Electrical, Electronic and Information Engineering, University di Bologna, I-40126 Bologna, Italy (e-mail: lorenzo.cavallucci3@unibo.it).

Giovanni Mangiulli is with the Dipartimento Energia "Galileo Ferraris", MAHTEP Group, Politecnico di Torino, I-10138 Torino, Italy (e-mail: giovanni.mangiulli@polito.it).

Michela Bracco and Laura Savoldi are with the Dipartimento Energia "Galileo Ferraris", MAHTEP Group, Politecnico di Torino, I-10138 Torino, Italy, and also with the Istituto Nazionale di Fisica Nucleare, Sez. di Genova, I-6146 Genova, Italy (e-mail: michela.bracco@ge.infn.it; laura.savoldi@polito.it).

Stefania Farinon and Riccardo Musenich are with the Istituto Nazionale di Fisica Nucleare, Sez. di Genova, I-6146 Genova, Italy (e-mail: stefania.farinon@ge.infn.it; riccardo.musenich@ge.infn.it).

Color versions of one or more figures in this article are available at https://doi.org/10.1109/TASC.2026.3655642.

Digital Object Identifier 10.1109/TASC.2026.3655642

© 2026 The Authors. This work is licensed under a Creative Commons Attribution 4.0 License. For more information, see https://creativecommons.org/licenses/by/4.0/

TABLE I
CABLE LAYOUTS

	Reference Design	Alternative Design	Return Cable
No. of MgB_2 wires	42	42	-
Former radius	8.2 mm	-	46 mm
Insulation thickness	2.5 mm	2.8 m	2.3 mm
Cable outer radius	13 mm	8 mm	50 mm

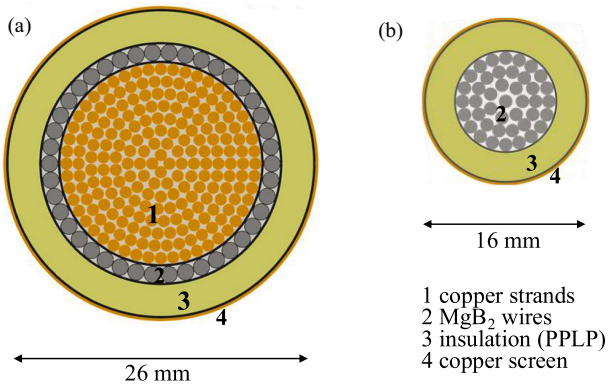


Fig. 1. (a) the MgB_2 wires are arranged around a former and assembled with highly conductive metal wires and (b) the MgB_2 wires are arranged in a bundle without a copper former.

located 30 m away from the MgB_2 line. The second layout is also a bipole line with a normal-conducting return, but it includes also an additional normal-conducting backup cable connected in parallel to the superconducting one. Also in this case, both the return and the backup lines are assumed 30 m from the MgB_2 line. The rationale of this backup cable is to protect the superconducting one during the electric fault.

Both cable configurations and line layouts are analyzed during a pole-to-ground electric fault.

II. CABLE AND MV-LINE LAYOUT

A. Cable Layouts

Magnesium diboride (MgB_2) is an excellent superconducting material for low magnetic field applications due to its high critical temperature (39 K) [14], its relatively low cost with respect to high temperature superconductors and to the availability of wires lengths of several kilometers [15], [16].

Two designs of an MgB_2 cable for the 300 MW line are here investigated during a fault. As mentioned before, the cable layout with the copper former is the nominal configuration, while the layout without former is proposed to reduce the cable cost. Both configurations can operate up to a temperature of 29 K with an I/Ic ratio of 90%. The main geometrical parameters of both cable designs are reported in Table I.

In the first layout, see Fig. 1(a), the MgB_2 wires are arranged around a bundle of highly-conductive metal wires (copper former) having the function of mechanical support and protection of the cable against over-currents. In total, 42-MgB_2 wires are arranged around a copper former with a diameter of 8.2 mm. This number of wires is set to guarantee an I/Ic ratio of 90%.

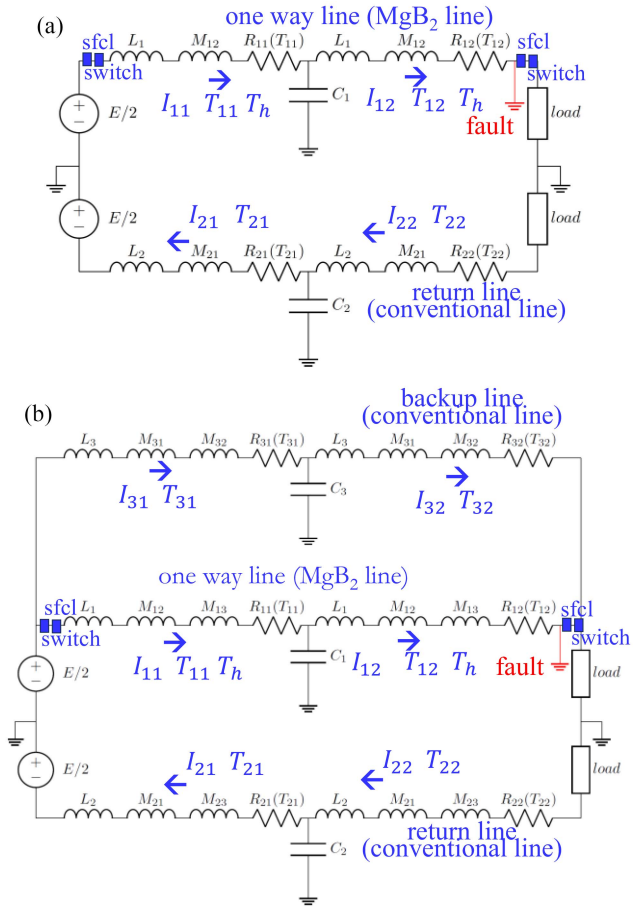


Fig. 2. Bipolar line layouts (a) with a conventional normal-conducting return, (b) with an additional normal-conducting backup cable in parallel with the superconducting one.

The former is designed to allocate the MgB_2 wires. The electrical insulation is provided by polypropylene laminated paper (PPLP) with an overall thickness of 2.5 mm. Several semiconductive layers, each with a thickness of less than 1 mm, are interposed between the copper former and the MgB_2-wires as well as between them and the insulation layer to avoid local electric charges deposition. A thin copper screen is grounded to null electric potential. The diameter of the cross-section of the SC cable, up to the copper screen, is 2.6 cm. This cable layout is referred to as the reference design, and it is the final design of the project.

In the second layout, see Fig. 1(b), the 42-MgB_2 wires are arranged in a bundle without a copper former. The electrical insulation is provided by polypropylene laminated paper (PPLP) with an overall thickness of 2.8 mm. The cable has a diameter of 1.6 cm.

B. MV-Line Layouts

Two possible layouts of the MV line have been analyzed in this work. The first configuration is a bipolar line with a conventional normal-conducting return, see Fig. 2(a), as already shown in [7] The second configuration, shown in Fig. 2(b), includes the

same arrangement but with an additional normal-conducting backup cable connected in parallel with the superconducting one. The rational of this backup cable is to protect the superconducting one during the electric fault. Both line configurations are connected to a superconducting fault current limiter and DC switches (Fig. 2). The superconducting fault current limiter is designed with a critical current that is 20% higher than the nominal operating current of the line. Its resistance in the non-superconducting state is 0.2 Ω.

III. Model Description

In this work a model that can be applied during the design phase of a superconducting line and that is able to estimate coupled electrical, thermal and fluid-dynamic phenomena is developed. The discretization of the line in two branches and the isochoric approximation of the hydraulic model, see next sections, represent the best compromise between accuracy and computational time.

A. Electric Model

To model a pole-to-ground short-circuit in the MV line, an electrical lumped-parameter "T" model of the line was developed. Each branch of the line (direct, return, or backup) is discretized into two sections. The model accounts for the self and mutual inductances of the line, the capacitance to ground of the cable, and the resistance of the conductors, see Table I.

The equations solved in the lumped electrical model are shown in (1) to (6) for the layout without backup branch. In case of the backup branch, a similar set of equations with the additional branch in parallel was solved

$$L_1\frac{dI_{11}}{dt}+M_{12}\frac{dI_{21}}{dt}=-(R_{11}(T_{11})+R_{\text{fcl}}(t))I_{11}+ -V_{C1}+\delta_{sw}\frac{E}{2} \quad (1)$$

$$L_1\frac{dI_{12}}{dt}+M_{12}\frac{dI_{22}}{dt}=-(R_{12}(T_{12})+R_{\text{fcl}}(t)) I_{12}-\delta R_{ld}I_{12}+V_{C1} \quad (2)$$

$$L_2\frac{dI_{21}}{dt}+M_{21}\frac{dI_{11}}{dt}=-R_{21}(T_{21})I_{21}-V_{C2}+\frac{E}{2} \quad (3)$$

$$L_2\frac{dI_{22}}{dt}+M_{21}\frac{dI_{12}}{dt}=-R_{22}(T_{22})I_{22}-R_{ld}I_{22}+V_{C2} \quad (4)$$

$$C_1\frac{dV_{c1}}{dt}=I_{11}-I_{12} \quad (5)$$

$$C_2\frac{dV_{c2}}{dt}=I_{21}-I_{22} \quad (6)$$

where $L_i[\text{H}]$ represents the self-inductance of a section of the line (see the sketch in Fig. 2), $M_{ij}[\text{H}]$ the mutual-inductance coupling between different sections, $C_i[\text{F}]$ the capacitance to ground of the cable section, see Table II, E the DC supply voltage, $I_{ij}[A]$ the current section, $R_{ld}[\Omega]$ the resistance of the load, δ a step function that is set to one before the fault and to zero at and after the fault event, δ_{sw} a similar step function to simulate the switch intervention, $R_{\text{fcl}}(t)[\Omega]$ the time-dependent resistance of the fault current limiter, $R_{ij}(T_{ij})[\Omega]$ the resistance of the line section computed as a parallel of the different layers that compose the cable. The MgB_2 is modelled with power law. The scaling law of the MgB_2 and its parameters as a function of temperature and magnetic flux density is presented in [17]. This fitting is obtained from experimental data.

TABLE II
Line Parameters

MgB_2 cable design with copper former					
l_1	2.0 μH/m	l_2	1.9 μH/m	l_3	1.9 μH/m
m_{12}	0.3 μH/m	m_{21}	0.3 μH/m	m_{31}	0.3 μH/m
C_1	5.9 nF	C_2	1.3 nF	C_3	1.3 nF
MgB_2 cable design with/o copper former					
l_1	2.1 μH/m	l_2	1.9 μH/m	l_3	1.9 μH/m
m_{12}	0.3 μH/m	m_{21}	0.3 μH/m	m_{31}	0.3 μH/m
C_1	10.0 nF	C_2	1.3 nF	C_3	1.3 nF

* values of self and mutual inductances are in μH/m

In the lumped electric circuit model, the resistance of the cable section $R_{ij}(T_{ij})$ is a function of the line-section temperature T_{ij} and it is computed as the parallel between the superconducting part ($R_{sc,ij}$) and the resistive one ($R_{cu,ij}$). Solving a non-linear relation allows to compute the current redistribution between the MgB_2 wires ($I_{sc,ij}$) and the copper former ($I_{cu,ij}$).

B. Thermal Model

The thermal model, see equations (7) to (10), accounts for the thermal inertia, the convection transfer to the hydrogen and the joule losses in the cable. The thermal conduction is neglected.

$$AL\rho C_p\frac{dT_{11}}{dt}=R_{sc11}I_{sc11}^2+R_{cu11}I_{cu11}^2-hA_w(T_{11}-T_H) \quad (7)$$

$$AL\rho C_p\frac{dT_{12}}{dt}=R_{sc12}I_{sc12}^2+R_{cu12}I_{cu12}^2-hA_w(T_{12}-T_H) \quad (8)$$

$$AL\rho C_p\frac{dT_{21}}{dt}=R_{cu21}I_{21}^2 \quad (9)$$

$$AL\rho C_p\frac{dT_{22}}{dt}=R_{cu22}I_{22}^2 \quad (10)$$

where $T_{ij}[\text{K}]$ is the temperature in the line section, see Fig. 2, $A[\text{m}^2]$ the cross-section of the cable, $L[\text{m}]$ the length of each breanch, $\rho[\text{kg/m}^3]$ and $C_p[\text{J/kgK}]$ respectively the homogenized density and specific heat of the cable, T_H the hydrogen temperature, $h[\text{W/m}^2\text{K}]$ the convection heat transfer coefficient, $A_w[\text{m}^2]$ the wetted area of the cable, $R_{sc,ij}[\Omega]$ the resistance of the superconducting portion of the SC cable, $R_{cu,ij}[\Omega]$ the resistance of the copper-part of the SC cable or the resistance of the normal-conducting cables (return or backup branches). A similar set of equations was solved in the presence of a backup branch.

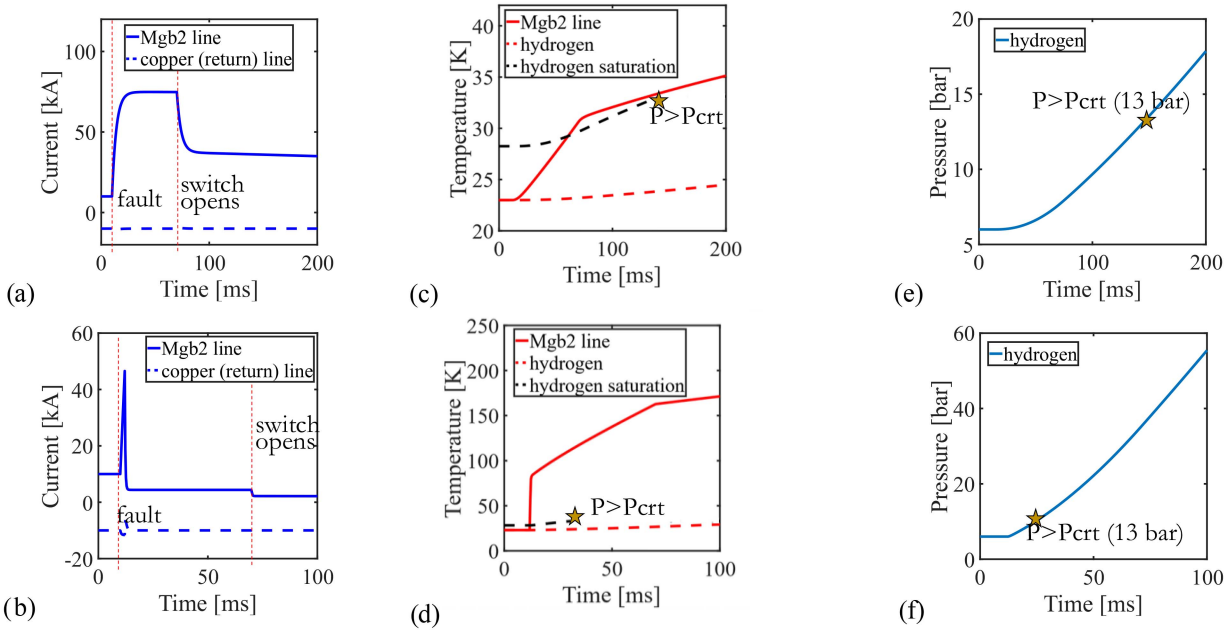


Fig. 3. Result of the pole-to-ground fault in the bipolar line with a *conventional normal-conducting return* in case of superconducting cable with and without copper former; (a) and (b) current in the MgB_2 line and in normal-conducting return line, respectively SC cable with (a) and with/o copper former (b); (c) and (d) temperature in the MgB_2 line, hydrogen temperature and hydrogen saturation temperature, SC cable respectively with (c) and with/o (d) copper former; (e) and (f) hydrogen pressure, SC cable respectively with (e) and with/o (f) copper former.

C. Hydraulic Model

The hydrogen temperature is computed by solving the energy conservation equation of the fluid, see (11), assuming an isochoric approximation (constant specific volume, see (12)).

$$V_H \rho_H C_{vH} \frac{dT_H}{dt} = hA_w \left(T_{11} - T_H\right) + hA_w \left(T_{12} - T_H\right) \tag{11}$$

$$\rho_H \left(T_H, P\right) = \text{constant} \tag{12}$$

where V_H is the hydrogen volume in the line, A_w the wetted surface, ρ_H and $C_{v,H}$ the respectively the density and specific volume of hydrogen and P the hydrogen pressure. The heat removed from the cable by convection, see in the r.h.s of (7) and (8), enters the fluid, see in the r.h.s of (11), to satisfy the heat balance. This isochoric simplification is valid under a fast transient that involves all the line, such as that occurring during a short circuit. The convection heat transfer coefficient h is computed from the Dittus-Boelter correction (13) for the Nusselt number Nu, resulting in a value of $\sim 500\ \mathrm{W/m^2K}$.

$$Nu = \frac{hD_h}{k} = 0.023 Re(T_H, P, v)^{0.8} Pr(T_H, P, v)^{0.3} \tag{13}$$

In (13), D_h is the hydraulic diameter of the LH2 channel, k is the fluid thermal conductivity, Re and Pr are the Reynolds and Prandtl number respectively and, v is the fluid velocity, computed from nominal hydrogen mass-flow rate in the line (1 kg/s), with a flow velocity in the range 0.8–1.5 m/s [10].

IV. Results and Discussion

A pole-to-ground fault condition is simulated in four different cases. The fault happens at $t = 0.5$ s. The response time of the DC switches is estimated in 60 ms (a conservative assumptions). A fast-acting solid-state DC circuit breaker (SSCB), representative of commercially available power-electronic-based protection devices in medium-voltage DC applications is assumed [18], [19].

Figs. 3 and 4 show the current in the MgB_2 line (I_{11} and I_{12} are approximatively equal), in the normal-conducting return cable ($I_{21} \approx I_{22}$) and in the backup lines ($I_{31} \approx I_{32}$), as well as the temperature in the MgB_2 line ($T_{11} \approx T_{12}$), the hydrogen temperature (computed at the pressure reached during the fault) and pressure for the four different cases discussed below:

1) MV bipolar line with a conventional normal-conducting return and SC cable with copper former, see Fig. 3(a), (c) and (e).
2) MV bipolar line with a conventional normal-conducting return and SC cable with/o copper former, see Fig. 3(b), (d) and (f).
3) MV bipolar line with a conventional normal-conducting return, backup branch and SC cable with copper former, see Fig. 4(a), (c) and (e).
4) MV bipolar line with a conventional normal-conducting return, backup branch and SC cable with/o copper former, see Fig. 4(b), (d) and (f).

In *case* 1 (no backup branch and SC cable with copper former, see Figs. 1(a) and 2(a)), the lower resistance of the SC cable, due to the copper former, results in a high short circuit current (up to 70 kA), see Fig. 3(a). However, the higher thermal inertia of the

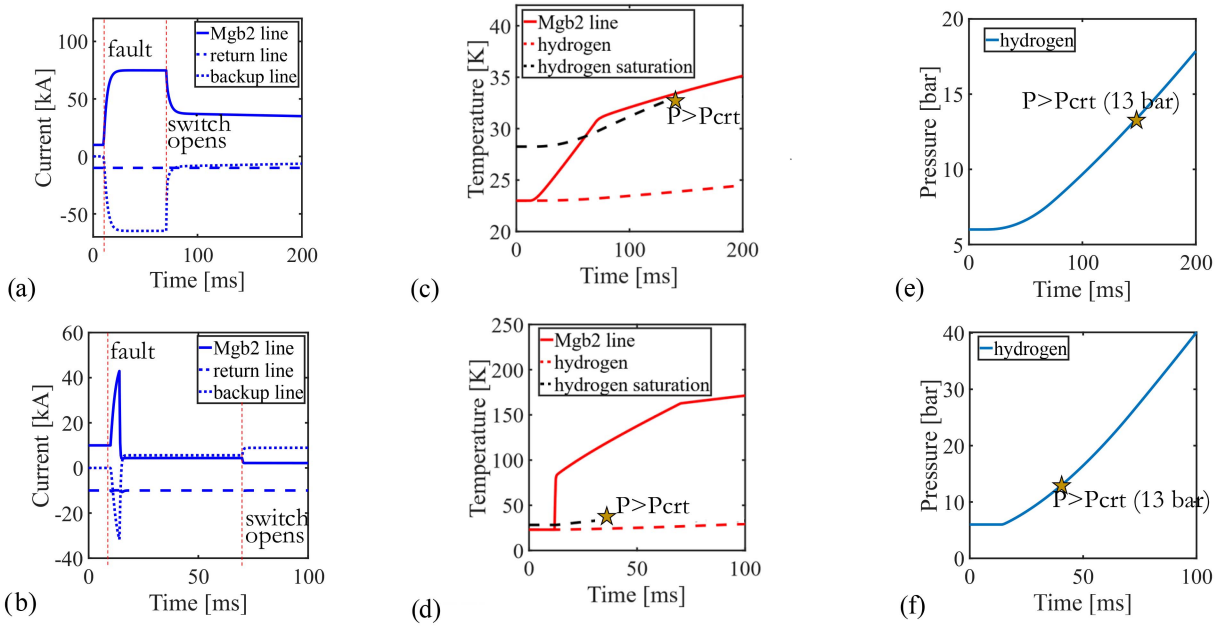


Fig. 4. Result of the pole-to-ground fault in the bipolar line with a *conventional normal-conducting return and backup line* in case of superconducting cable with and without copper former; (a) and b) current in the MgB_2 line and in normal-conducting return line, respectively SC cable with (a) and with/o copper former (b); (c) and (d) temperature in the MgB_2 line, hydrogen temperature and hydrogen saturation temperature, respectively SC cable with (c) and with/o (d) copper former; (e) and (f) hydrogen pressure, respectively SC cable with (e) and with/o (f) copper former.

cable allows to limit the hot-spot temperature of the cable below 35 K, see Fig. 3(c). The hydrogen temperature (dotted line) remains below the saturation temperature, so no fluid boiling occurs.

In *case* 2 (no backup line and SC cable with/o a copper former, see Figs. 1(b) and 2(a)), the higher electrical resistance of the cable limits the overcurrent to about 40 kA. During the fault, the transition of the MgB_2 wires further increases the cable resistance, reducing the short circuit current before the switch intervention. However, due to the lower thermal inertia, the SC cable reaches a hot-spot temperature above 100 K, and the hydrogen temperature is close to the saturation point before the switch intervention, see Fig. 3(d). This results in a more critical situation for the line. The higher hydrogen temperature also causes a higher hydrogen pressurization up to about 40 bar. In this case, prompt intervention of the relief valves is required and the possibility of a mechanical failure of the cryostat has to be verified.

In *case* 3 (with backup line and SC cable with copper former, see Figs. 1(a) and 2(b)) the results are similar to those discussed in *case* 1. The overcurrent reaches about 70 kA, see Fig. 4(a), and the hydrogen temperature remains below the saturation temperature, see Fig. 4(c). It is worth noting that during the fault, before the switch intervention, the overcurrent in the SC line flows into the backup line. The same overcurrent (with negative sign) is observed in the backup line. This behaviour is specific to the fault condition analysed here. In fact, in the pole-to-ground fault shown in Fig. 2(b), before the switch intervention, both the SC and the backup branches are connected to the ground, that works as a common node, and are in fault condition. The current can consequently flow from the MgB_2 line to the backup line. Once the switches are open, the backup line is disconnected from the ground and resumes normal operation. During the transient, the current continues flowing until the energy stored in the inductances is completely discharged. These results show that the backup line does not have a significant impact on either the overcurrent or the hot-spot temperature during a short circuit. A proper switch intervention is important also in this case, since the backup line does not provide self-protection during a fault.

In *case* 4 (with backup line and SC cable with/o copper former, see Figs. 1(b) and 2(b)) the same observation made for *case* 2 can be applied. The higher resistance of the SC cable limits the short-circuit current, see Fig. 4(b). However, the lower thermal inertia results in a higher hot-spot temperature, reaching values close to the hydrogen saturation temperature, see Fig. 4(d). This condition creates a potentially dangerous operating condition for the line. During the fault, the hydrogen pressure rises up to 30 – 40 bar, requiring proper activation of the relief valves to prevent possible mechanical damage to the cryostat [7], [10].

V. Conclusion

The fault conditions in a 300 MW, 30 kV DC line have been analysed with a simplified lumped-parameter electrical model, coupled with a thermal model and a hydraulic model. The model simplifications allow a relatively fast calculation of off-normal conditions, that proves the model a useful tool during the design phase of the cable configuration and line layout.

Two cable designs are investigated. In the first one, the final layout of the project, MgB_2 wires are arranged around a former and assembled with highly conductive metal wires. In the second one, the former is absent. The line is designed as a bipole

one with a conventional normal-conducting return. This is the reference design of the project. In a second tentative layout, an additional backup normal-conducting branch is added in parallel to the superconducting one.

The results of the fault conditions show that the cable design with/o a copper former limits the short circuit current due to the higher resistance of the cable. However, because of its lower thermal inertia, the cable reaches a higher temperature during the fault. Although the design without the former limits the short-circuit current, it is not recommended.

The line layout with the backup branch does not show any significant impact on the short-circuit current, and the backup line is not self-protecting, requiring a prompt switch intervention. However, the backup line plays a role during maintenance of the line, and it generally increases the overall system reliability when the superconducting line needs to be disconnected. The trade-off between the additional cost of the backup line and its advantages for the system reliability should be properly assessed for each specific application.

ACKNOWLEDGMENT

This manuscript reflects only the authors' views and opinions, and the Ministry cannot be considered responsible for them.

REFERENCES

[1] M. Tropeano et al., "Progress in MgB_2 wires manufacturing at ASG superconductors and perspective for applications," *IEEE Trans. App. Supercond.*, vol. 35, no. 5, Aug. 2025, Art. no. 6200107.

[2] T. Spina et al., "Recent development and status of ex-situ PIT MgB_2 wires at ASG superconductors," *IEEE Trans. App. Supercond.*, vol. 34, no. 3, May 2024, Art. no. 6200304.

[3] L. Fu et al., "Hydrogen-electricity hybrid energy pipelines for railway transportation: Design and economic evaluation," *Int. J. Hydrogen Energy*, vol. 61, pp. 251–264, 2024.

[4] L. Savoldi, A. Balbo, C. E. Bruzek, G. Grasso, M. Patti, and M. Tropeano, "Conceptual design of a SuperConducting energy pipeline for LH_2 and power transmission over long distances," *IEEE Trans. Appl. Supercond.*, vol. 34, no. 3, May 2024, Art. no. 5400805.

[5] J. Yang et al., "Roadmap to offshore power-liquid hydrogen co-production and hybrid delivery system based," *Energy Proc.*, vol. 41, 2024, Art. no. 10965.

[6] C. E. Bruzek et al., "MgB_2-Based MVDC superconducting power cable in liquid hydrogen for hybrid energy distribution," *IEEE Trans. Appl. Supercond.*, vol. 34, no. 3, May 2024, Art. no. 6200405.

[7] M. Bracco et al., "Desing od a submarine 30-km MgB_2 cable for the combined transfer of 0.3 GW_e and LH_2 from offshore plants to the Ravenna Port," *IEEE Trans. Appl. Supercond.*, vol. 35, no. 5, Aug. 2025, Art. no. 5400906.

[8] 2024. Accessed: Sep. 16, 2024. [Online]. Available: https://www.agnespower.com/

[9] G. Mangiulli et al., "Sizing and economic assessment for auxiliar components and grid connection of a MgB_2-LH_2 hybrid power cable," *IEEE Trans. Appl. Supercond.*, early access, Jan. 05, 2026, doi: 10.1109/TASC.2026.3651232. [Online]. Available: https://ieeexplore.ieee.org/abstract/document/11329181

[10] L. Savoldi et al., "Analysis of the evolution of accidental transients in the cooling of a MgB_2-LH_2 hybrid power cable," *IEEE Trans. Appl. Supercond.*, 2025. [Online]. Available: https://ieeexplore.ieee.org/abstract/document/11329175

[11] S. Palacios et al., "Design of a 75 km GW-class hybrid pipeline for the synergetic transmission of liquid hydrogen and electrical energy by high-temperature superconductivity," *Supercond. Sci. Technol.*, vol. 38, no. 12, 2025, Art. no. 125025, doi: 10.1088/1361-6668/ae2cf7.

[12] C. Creusot et al., "Superconducting cable modelling into electro- magnetic transient simulation tool," *IEEE Trans. Appl. Supercond*, vol. 34, no. 3, May 2024, Art. no. 5400606, doi: 10.1109/TASC.2024.3370118.

[13] W. de Sousa, "Transient simulations of superconducting fault current limiters," Ph. D. dissertation, Dept. Elect. Eng, Federal Univ. Rio de Janeiro, Rio de Janeiro, Brazil, 2015.

[14] L. Soldati et al., "Numerical and experimental investigation of AC losses in MgB_2 wires," *Supercond. Sci. Technol.*, vol. 38, no. 6, 2025, Art. no. 065019.

[15] S. Kloppel et al, "Thermo-hydraulic and economic aspects of long-length high-power MgB_2 superconducting cables," *Cryogenics*, vol. 113, 2021, Art. no. 103211.

[16] L. Cavallucci et al., "Optimization procedure to design a DC transmission line with MgB_2 wires in liquid hydrogen," *IEEE Trans. Appl. Supercond.*, vol. 35, no. 5, Aug. 2025, Art. no. 5400205.

[17] L. Soldati, M. Breschi, P. L. Ribani, T. Spina, and C.-É. Bruzek, "AC loss investigation in MgB_2 multifilamentary wires: A numerical study," *IEEE Trans. Appl. Supercond.*, vol. 34, no. 3, May 2024, Art. no. 6200805.

[18] A. Kaharević et al., "A review of HVDC and MVDC grid protection," in *Proc. 19th Int. Conf. AC DC Power Transmiss.*, Glasgow, U.K., 2023, pp. 271–280.

[19] P. Dworakowski et al., "Protection of radial MVDC electric network based on DC circuit breaker and DC fuses," *Int. J. Elect. Power Energy Syst.*, vol. 153, 2023, Art. no. 109398.

Open Access funding provided by 'Alma Mater Studiorum - Università di Bologna-2025-2027 Deposit account' within the CRUI CARE Agreement